

A method for simple and accurate estimation of fog deposition in a mountain forest using a meteorological model

Genki Katata,¹ Mizuo Kajino,² Takatoshi Hiraki,³ Masahide Aikawa,³ Tomiki Kobayashi,³ and Haruyasu Nagai¹

Received 24 December 2010; revised 25 July 2011; accepted 26 July 2011; published 18 October 2011.

[1] To apply a meteorological model to investigate fog occurrence, acidification and deposition in mountain forests, the meteorological model WRF was modified to calculate fog deposition accurately by the simple linear function of fog deposition onto vegetation derived from numerical experiments using the detailed multilayer atmosphere-vegetation-soil model (SOLVEG). The modified version of WRF that includes fog deposition (fog-WRF) was tested in a mountain forest on Mt. Rokko in Japan. fog-WRF provided a distinctly better prediction of liquid water content of fog (LWC) than the original version of WRF. It also successfully simulated throughfall observations due to fog deposition inside the forest during the summer season that excluded the effect of forest edges. Using the linear relationship between fog deposition and altitude given by the fog-WRF calculations and the data from throughfall observations at a given altitude, the vertical distribution of fog deposition can be roughly estimated in mountain forests. A meteorological model that includes fog deposition will be useful in mapping fog deposition in mountain cloud forests.

Citation: Katata, G., M. Kajino, T. Hiraki, M. Aikawa, T. Kobayashi, and H. Nagai (2011), A method for simple and accurate estimation of fog deposition in a mountain forest using a meteorological model, *J. Geophys. Res.*, *116*, D20102, doi:10.1029/2010JD015552.

1. Introduction

[2] Mountain forests are important sinks for trace gases and particles, such as nitrogen and sulfur compounds as well as photochemical oxidants. The deposition flux of these compounds over forests is a major contributor to ecosystem acidification and eutrophication [Alewell *et al.*, 2000; Conley *et al.*, 2009]. Numerous studies of atmospheric transport and deposition have been conducted to determine the importance of surface removal, better known as wet, dry and fog (cloud water) deposition by measurements and models [Hicks *et al.*, 1991; Wesely, 1989; Erisman, 1994; Erisman *et al.*, 1997, 1998; Choularton *et al.*, 1997; Wesely and Hicks, 2000]. In particular, fog deposition significantly contributes to hydrological, nutrient and pollutant inputs in such mountainous regions. This is because high concentrations of solutes in fog water lead to fog deposition of these substances that can be as high as or higher than dry or wet deposition [Igawa *et al.*, 2002; Herckes *et al.*, 2002; Lange *et al.*, 2003]. The quantification of fog deposition onto forest canopies in mountainous areas is, therefore, of interest in terms of its effect on forest health and decline.

[3] Wet deposition associated with the process of precipitation can be readily estimated from precipitation and scavenging rates. In contrast, dry and fog depositions on land surfaces are associated with the turbulent exchange of gas, particles and fog droplets, which are more complicated since they are affected by many environmental factors such as meteorology and surface characteristics [Lovett and Kinsman, 1990]. Numerous one-dimensional dry deposition models have therefore been developed based on the analogy of electrical current flowing through a network of resistances to quantify the amount of dry deposition [e.g., Wesely, 1989; Hicks *et al.*, 1991; Meyers *et al.*, 1998; Pleim *et al.*, 2001; Zhang *et al.*, 2001, 2002, 2003; Wu *et al.*, 2003]. When incorporated into three-dimensional chemical transport models (CTMs), these deposition models are useful tools for predicting the horizontal distribution of deposition flux over terrestrial surfaces.

[4] In contrast to dry and wet deposition, however, numerical studies for fog deposition using the meteorological models and CTMs have been rarely employed in mountainous regions, and are not successful in reproducing or predicting fog occurrence or acidification in such regions. Recent studies revealed that meteorological models and CTMs frequently failed to predict the liquid water content of fog (LWC) and ionic concentrations in fog water. Meteorological models successfully simulated general trends of observed fog events, but substantially overestimated the LWC over mountain forests [Katata *et al.*, 2010]. This overestimation causes an underestimation of ionic concentrations in fog by CTMs [Shimadera *et al.*, 2009] and probably leads to large errors in

¹Japan Atomic Energy Agency, Tokai, Japan.

²Meteorological Research Institute, Tsukuba, Japan.

³Hyogo Prefectural Institute of Environmental Sciences, Kobe, Japan.

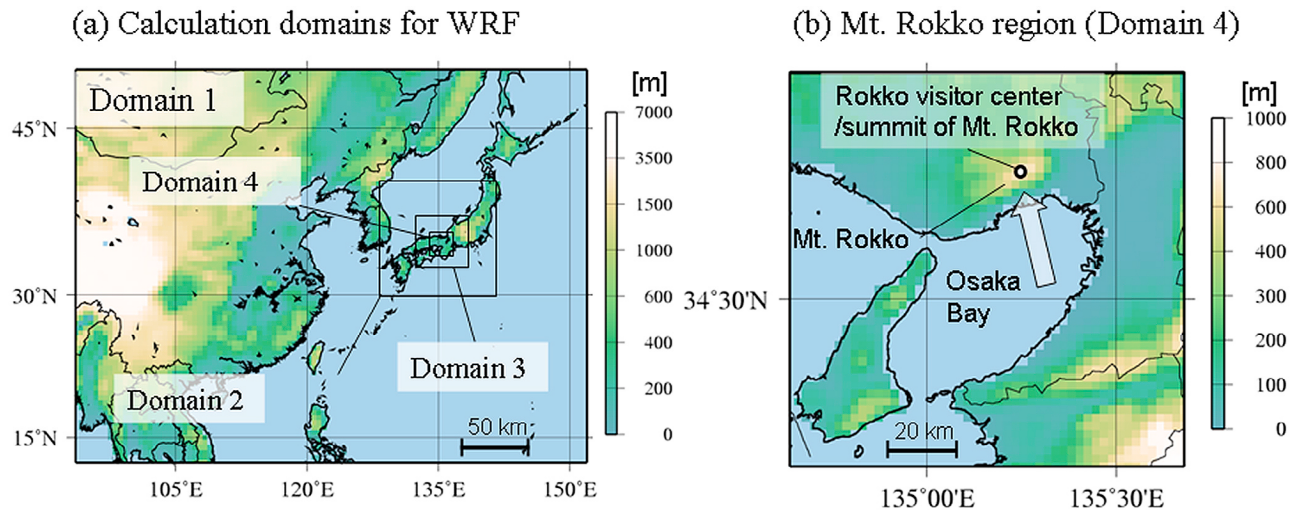


Figure 1. (a) Topographical maps of domain 1 and (b) of the region around Mt. Rokko in domain 4 for WRF calculations. The simulation grid that includes both the Rokko Visitor Center and the summit of Mt. Rokko is plotted in Figure 1b. The arrow in Figure 1b shows the dominant wind that flow to Mt. Rokko in the simulation period.

predicting acid fog deposition in mountain forests. Among the possible reasons for this suggested by *Katata et al.* [2010], the most significant one is thought to be the lack of a process for removing fog or cloud droplets by forest canopies (i.e., fog deposition) in current meteorological models and CTMs. A meteorological model that includes the process of fog deposition onto vegetation is therefore needed to ensure an accurate prediction of LWC in mountain forests.

[5] One-dimensional fog deposition models proposed by *Slinn* [1982] and *Lovett* [1984] have been widely used to estimate fog deposition onto forest canopies. Their performance in predicting measured fog deposition flux over vegetative surfaces has, however, only been evaluated with a limited data set [*Katata et al.*, 2008]. *Klemm et al.* [2005] suggested that, in fact, the widely used fog deposition model by *Lovett* [1984] overestimates the measured fog deposition flux over forest canopies by up to 32%. This overestimation would very likely result in significant errors that would hinder the accurate prediction of fog deposition over a coniferous forest. From such a background, the following simple linear equation of fog deposition velocity, V_d , has been proposed by *Katata et al.* [2008]:

$$V_d = AU, \quad (1)$$

where A is the slope of V_d that depends on vegetation characteristics (nondimensional), and U the horizontal wind speed over forest canopies [m s^{-1}]. The simple formulation of equation (1) based only on horizontal wind speed has been derived from numerical experiments using a detailed multi-layer land surface model that includes fog deposition onto vegetation (SOLVEG) [*Katata et al.*, 2008]. Equation (1) makes it possible to readily estimate fog deposition with little prediction error and is suitable for incorporation into the meteorological model. However, the parameters used in equation (1) have been set for coniferous forests in Germany, and may be inadequate for different ambient meteorological conditions (e.g., air temperature and humidity). The perfor-

mance of meteorological models that include equation (1) should therefore be tested in some environments to estimate fog deposition in the world's cloud forests.

[6] The aim of the present study is to incorporate the scheme of fog deposition onto vegetation into a state-of-the-art meteorological model. The meteorological model of Advanced Research WRF [*Skamarock et al.*, 2008] was modified to calculate the removal of cloud (fog) liquid water on the ground surface due to fog deposition based on equation (1). The performance of the modified WRF model in predicting LWC and fog deposition was validated by comparing with estimated fog deposition derived from throughfall observations under coniferous trees at the Rokko Visitor Center near the summit of Mt. Rokko in Japan. To confirm the performance of equation (1) under climatic conditions in East Asia, calculations using the modified WRF model were compared with those using the detailed fog deposition model SOLVEG. Finally, fog deposition onto forest canopies on Mt. Rokko was estimated by numerical simulation.

2. Numerical Models

2.1. Meteorological Model: WRF

[7] The authors employed a simulation of Advanced Research WRF (Weather Research and Forecasting) Version 3.1 to reproduce fog episodes in a mountain forest. This has various options for parameterizations of turbulence, grid-resolved and unresolved cloud processes, and radiation, as well as coupling to land surface models. Four nested computational domains were used in this study (Figure 1), with a horizontal grid of 105×81 , 73×73 , 100×100 and 127×127 cells and mesh sizes of 54, 18, 6 and 2 km, respectively, and 28 vertical layers from the surface up to 100 hPa. A one-way nesting interaction without feedback from the child domain to the mother domain was used.

[8] The physical parameterizations of WRF used in this study are summarized in Table 1. The WRF Single-Moment 6-class scheme (WSM6) [*Hong and Lim*, 2006] was selected

Table 1. Model Settings for WRF Used in the Present Study

	Domain 1	Domain 2	Domain 3	Domain 4
Horizontal grid cell	105 × 81	73 × 73	100 × 100	127 × 127
Spatial resolutions	54 km	18 km	6 km	2 km
Time step	300 s	100 s	33 s	11 s
Vertical levels ^a	28	28	28	28
Nesting option	One-way	One-way	One-way	One-way
Boundary and initial conditions	JRA-25 ^b + ERA-40 ^c			
Sea surface temperature	OI-SST ^d	OI-SST ^d	OI-SST ^d	OI-SST ^d
Time step	Included	None	None	None
Physical parameterizations				
Cumulus	BMJ ^e	BMJ ^e	None	None
Cloud microphysics	WSM6 ^f	WSM6 ^f	WSM6 ^f	WSM6 ^f
Radiation	RRTM ^g + Dudhia ^h			
Planetary boundary layer	MYNN 2.5 ⁱ	MYNN 2.5 ⁱ	MYNN 2.5 ⁱ	MYNN 2.5 ⁱ
Land surface	Noah LSM ^j	Noah LSM ^j	Noah LSM ^j	Noah LSM ^j

^aTerrain-following sigma levels from surface to 100 hPa as 1.00, 0.99, 0.978, 0.964, 0.946, 0.922, 0.894, 0.86, 0.817, 0.766, 0.707, 0.644, 0.576, 0.507, 0.444, 0.38, 0.324, 0.273, 0.228, 0.188, 0.152, 0.121, 0.093, 0.069, 0.048, 0.029, 0.014, and 0.00.

^bJapanese 25-year Reanalysis (horizontal resolution: 2.5° × 2.5°) for atmosphere.

^cECMWF 40-year Reanalysis (horizontal resolution: 2.5° × 2.5°) for soil temperature and moisture.

^dOptimum Interpolation Sea Surface Temperature.

^eJanjic [1994, 2000, 2002].

^fHong and Lim [2006].

^gMlawer et al. [1997].

^hDudhia [1989].

ⁱNakanishi and Niino [2004].

^jChen and Dudhia [2001].

for the grid-scale cloud microphysics model. The Mellor-Yamada Nakanishi-Niino (MYNN) model Level 2.5 [Nakanishi and Niino, 2004] was used for planetary boundary layer turbulence calculations. The Noah Land Use Model (Noah LSM) [Chen and Dudhia, 2001] was used for calculating heat and moisture exchanges at the land surface. Subgrid-scale cumulus convection was parameterized using the Betts-Miller-Janjic scheme [Janjic, 1994, 2000, 2002] for domains 1 and 2 with coarse grid size. Atmospheric radiative transfer was solved using the Rapid Radiative Transfer Model (RRTM) for long-wave radiation [Mlawer et al., 1997] and the Dudhia scheme [Dudhia, 1989] for short-wave radiation.

2.2. Incorporation of Fog Deposition Process Into the Meteorological Model

[9] As mentioned by Shimadera et al. [2009], the meteorological models and CTMs predicted LWC and ion concentrations in fog water with large errors. These are thought to have been caused by inappropriate calculations of fog deposition onto forest canopies in the models. Vertical mixing of cloud water is numerically calculated by solving the one-dimensional mass conservation equation of total liquid water content (specific humidity + LWC) in MYNN planetary boundary scheme [Nakanishi and Niino, 2004] in the WRF model. The equation consists of the following terms: advection, turbulent diffusion, evaporation/condensation, and gravitational settling and turbulent deposition of fog droplets. At the lowest atmospheric layer just above the ground surface, the flux of cloud (fog) water deposition, F_{qc} [$\text{kg m}^{-2} \text{s}^{-1}$], has an important role in the mass balance equation, which is modeled in MYNN scheme using the bulk transfer coefficient for heat and water vapor, c_h :

$$F_{qc} = c_h |\mathbf{u}| \rho q_c, \quad (2)$$

where ρ is the air density [kg m^{-3}], $|\mathbf{u}|$ and q_c are the horizontal wind speed [m s^{-1}] and the cloud water content

[kg kg^{-1}] at the lowest atmospheric layer (about 35 m in height), respectively. The elevation of $|\mathbf{u}|$ may be different from that of U in (1) in some case, but this does not cause a significant error in representative wind speed according to the logarithmic wind profile in the surface boundary layer. The deposition velocity of fog for forest canopies, V_d , is however usually 1–2 orders of magnitude larger than the so-called exchange velocity for heat and water vapor, $c_h |\mathbf{u}|$, because the collection efficiency of fog droplets by leaves due to the inertial impaction and gravitational settling is larger than the heat and water vapor exchanges determined by molecular diffusion coefficients and stomatal resistance over leaf surface. For example, $V_d = 0.12 \text{ m s}^{-1}$ [Katata et al., 2008] and $c_h |\mathbf{u}| \leq 0.01 \text{ m s}^{-1}$ [Kondo and Watanabe, 1992], with the use of $|\mathbf{u}| = 5 \text{ m s}^{-1}$ over forest canopies. Since LWC value at the lowest atmospheric layer is directly affected by the deposition flux (F_{qc}), this discrepancy probably causes an overestimation of LWC calculated by WRF model.

[10] To calculate fog deposition accurately, the authors modified WRF by replacing $c_h |\mathbf{u}|$ in equation (2) with V_d , using $|\mathbf{u}|$ instead of U in equation (1), rewritten as:

$$V_d = A |\mathbf{u}|, \quad (3)$$

$$A = 0.0164 (\text{LAI}/h)^{-0.5},$$

where LAI is the Leaf Area Index and h the canopy height [m]. The calculations of A using equation (3) agreed with observations in various cloud forests with $\text{LAI}/h > 0.2$ [Katata et al., 2008, Figure 11a]. The accuracy of equation (2) in the amount of fog deposition has been validated with data on turbulent fog flux over a coniferous forest in Germany [Klemm and Wrzesinsky, 2007] with a prediction error of 13%, clearly smaller than that of 32% when using the widely used multi-layer fog deposition model of Lovett [1984] [Katata et al., 2008]. The effect of fog deposition on LWC is discussed in section 4.1.

2.3. Multilayer Land Surface Model: SOLVEG

[11] The SOLVEG simulation was employed with the simulation grid of domain 4 in WRF that includes both the Rokko Visitor Center (135°13'45"E, 34°45'24"N, Figure 1b) and the summit of Mt. Rokko (135°14'52"E, 34°46'00"N, Figure 1b). The aim of SOLVEG calculations was to confirm the performance of the modified WRF model in predicting fog deposition onto vegetation under climatic conditions of East Asia. SOLVEG consists of one-dimensional multilayer submodels for the atmosphere near the surface, soil and vegetation interactions with a radiation transfer scheme used to calculate the transmission of solar and long-wave radiation fluxes in canopy layers. Schemes for the deposition of gaseous and particulate matters (including fog droplets) at each canopy layer were incorporated into the model and verified with flux data of gases (water vapor [Nagai, 2002, 2003; Katata et al., 2007], CO₂ [Nagai, 2005], and O₃ [Katata et al., 2011]) and particles (fog droplets [Katata et al., 2008] and aerosols [Katata et al., 2011]) measured by gradient and eddy covariance methods. Details of the model have been described by Nagai [2005] and Katata et al. [2008].

[12] The atmosphere submodel calculates atmospheric variables by numerically solving one-dimensional diffusion equations for horizontal wind speed components, potential temperature, specific humidity, liquid water content of fog, turbulent kinetic energy and length scale, and CO₂ concentration. The top boundary conditions are given from WRF output data in the present study. The boundary conditions of soil surface are the momentum, heat and water vapor fluxes calculated using bulk transfer equations of wind speed, potential temperature, and specific humidity at the lowest atmospheric layer and the soil surface temperature and specific humidity, determined via the soil submodel.

[13] The soil submodel computes the soil temperature, volumetric soil water content and specific humidity of air in the soil pore space using a heat conduction equation, a mass balance equation for liquid water and a diffusion equation for water vapor, respectively. These three equations are connected each other using a source term of evaporation or condensation rate in soil. The root uptake of soil water is calculated as being equal to the transpiration rate calculated in the vegetation submodel. The top of boundary conditions are given by solving heat and water budget equations at soil surface in the atmosphere submodel. The soil CO₂ exchanges due to the diffusive and convective transport of CO₂ in both aqueous and gas phases are included in the mass conservation of CO₂ for unsaturated soil.

[14] The vegetation submodel calculates the leaf temperature and water on the surface of leaves (leaf surface water) for each canopy layer, and the vertical liquid water flux in the entire canopy. The leaf temperature is derived from the heat budget equation at the leaf surface using the variables from the atmosphere and radiation submodel. The WRF output of precipitation intensity is used to the top boundary conditions of the vertical liquid water flux in the canopy. Then, the vertical liquid water flux at the bottom of the canopy is calculated based on the surface liquid water budget equation in the soil submodel. The CO₂ assimilation rate due to is photosynthesis calculated based on Farquhar's formulations [Farquhar et al., 1980] with use of the relation between the stomatal resistance and net CO₂ assimilation rate [Collatz et al., 1991, 1992].

[15] The radiation submodel calculates the direct and diffuse downward and upward fluxes of solar and long-wave radiation in the canopy to give the radiation energy input to the soil surface and vegetation canopy layers in the soil and vegetation submodels. The radiation budgets at each canopy layer are computed for both sunlit and shaded leaves. The stomatal resistance and energy budget are then calculated independently for each fraction.

[16] Iterative calculations are adapted to solve the equations numerically which are closely related to each other. A small time step applied to each simulation scenario is therefore used to reduce the iteration of the submodels and bring them within a single time step.

[17] The atmosphere and vegetation submodels include modules for calculating fog deposition onto leaves based on the processes of inertial impaction and gravitational settling of particles at each vegetation layer [Katata et al., 2008]. The schemes of collection rates due to Brownian diffusion and interception, which affect the deposition of fine particles typically smaller than 0.1 μm in diameter, have recently been incorporated in SOLVEG [Katata et al., 2011]. All collection processes of particles are formulated based on semiempirical equations obtained by wind-tunnel studies for packed fibers of a filter.

2.4. Simulation Conditions and Model Scenarios

[18] The boundary and initial conditions for the WRF simulations were obtained for every six hours using Japanese 25-year Reanalysis (JRA-25) data from 2.5 degrees at 17 pressure levels. The NOAA Optimum Interpolation Sea Surface Temperature (OI-SST) developed at the National Centers for Environmental Prediction/National Weather Service/National Oceanic and Atmospheric Administration (NCEP/NWS/NOAA) were used for the sea surface temperature. Soil temperature and moisture were initialized using ECMWF 40-year Reanalysis (ERA-40) data.

[19] It is impossible to know that the fog (or cloud) is present at the ground surface or at the lowest level of atmosphere since the WRF model does not distinguish both fog appearances in its calculations. In the present study, 'Fog' was thus simply defined in WRF simulations as being when visibility (VIS) was less than 1 km when LWC at the lowest level (about 35 m in height) of the atmosphere > 0.017 g m⁻³ experimentally obtained from the relationship for VIS and LWC by Kunkel [1984]. Calculations of LWC were compared with observations sampled using an active strand-fog collector placed at the Rokko Visitor Center (see section 3).

[20] In order to determine the upper boundary conditions of SOLVEG, hourly values for the various meteorological variables (horizontal wind speed, air temperature and humidity, short and long wave radiations, fog water content and precipitation) in the lowest atmospheric layer (about 35 m in height) were used from the grid that includes the Rokko Visitor Center and the summit of Mt. Rokko in domain 4 of WRF. Due to a lack of soil data, the initial conditions or soil temperature and volumetric soil water content were set as constant values of 15°C and 0.3 m³ m⁻³ for all soil layers. There were also no available data for vegetation parameters of LAI or canopy height for calculations using SOLVEG and equation (3) during the simulation period. Thus, observations of LAI and the canopy height of cedar trees were made at the

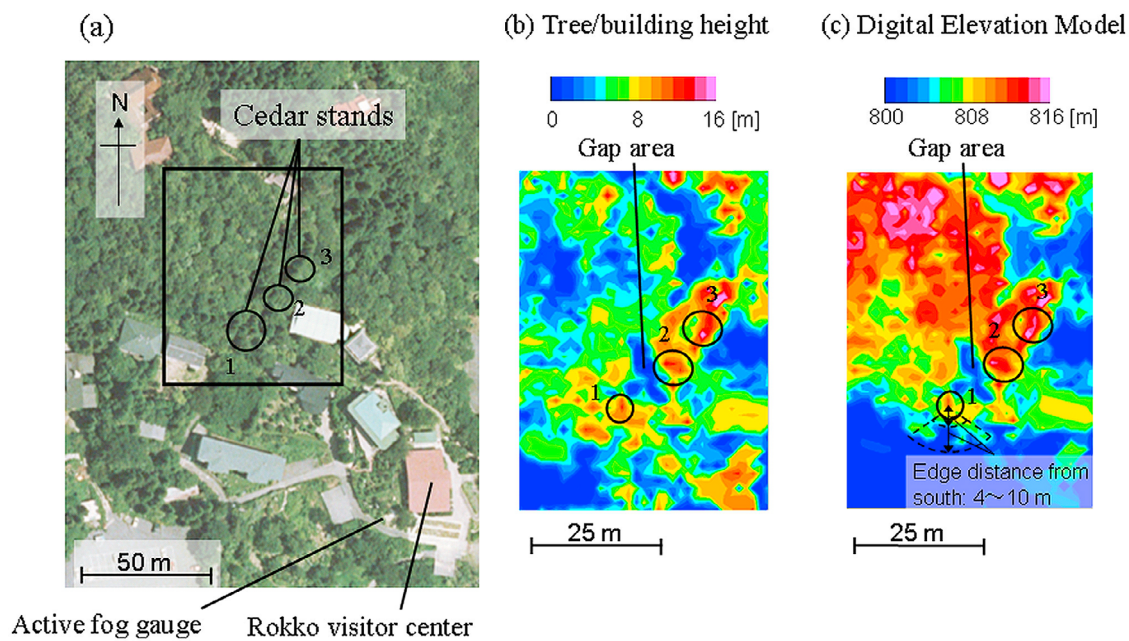


Figure 2. (a) A digital ortho image around the Rokko Visitor Center (Figure 1b) and (b) maps of tree or building height and (c) topography for the region surrounded by the square in Figure 2a derived from high-resolution GIS data measured by airborne laser scanner (LIDAR). Numbers in Figures 2b and 2c represent the cedar coniferous stands where throughfall observations were carried out. The products of the ortho image and the LIDAR were provided by Kokusai Kogyo Co., Japan.

Rokko Visitor Center (Figure 2a) using VERTEX IV Hypsometer (Haglof Co., Sweden) and LAI-2000 Plant Canopy Analyzer (LI-COR Co., USA) on 1 August 2009. Measured values of canopy height and LAI were 13 m and 4.5 ± 0.56 , respectively, and these were used as input data of SOLVEG and equation (3). From the above value of LAI, the uniform profile of Leaf Area Density (LAD) was given from 6 to 13 m in height, since vertical profiles of LAD had a small effect on fog deposition calculation according to the sensitivity test (results not shown here) using SOLVEG with some LAD profile patterns representing forest canopy structures. Root fractions at each soil depth were set at the homogeneous values of 0 to 0.5 m below the surface based on the common knowledge that the roots of most trees are distributed within the top 0.6 m of the soil profile [Crow, 2005]. SOLVEG uses the droplet size distribution function of fog water as the modified Gamma distribution by *Deirmendjian* [1969] with use of the mean droplet diameter (D_{mean} [μm]) being determined with the linear function of LWC as: $D_{\text{mean}} = 17.3 \times 10^3 \text{ LWC [g m}^{-3}] + 9.72$ [Katata *et al.*, 2008].

[21] WRF calculations were first used to simulate meteorological fields that included fog events for the study area. All calculations using the models were carried out for the period from 14 to 27 July 1999. The simulation was initialized by running WRF with 5 days as a spin-up time. In order to investigate the impact of fog deposition on LWC, two calculations using the WRF model were employed: one using the WRF revised to calculate fog deposition onto forest canopies as formulated by equation (3) (hereinafter referred to as ‘fog-WRF’), and the other using the original version of WRF (‘org-WRF’) based on the parameterization of the bulk exchange coefficient by equation (2). SOLVEG calculations were carried out using the output of meteorological

variables at the lowest atmospheric layer (approximately 35 m) by org-WRF and fog-WRF for the grid in the finest domain that included Mt. Rokko throughout the simulation period.

3. Study Area and Observational Data

[22] The study area was the Mt. Rokko region in Kobe Prefecture, Japan, located at an altitude of 800 m above sea level (Figure 1b). Mt. Rokko is subject to air pollutants transported from a highly industrialized area near the sea located to the south of the mountain (Figure 1b). This is one of just a few places in Japan where long-term observations in LWC have been carried out continuously since 1997.

[23] In the present study, the authors focused on fog events occurring on Mt. Rokko from 20 to 25 July 1999 [Kobayashi *et al.*, 2002]. For evaluation of WRF, fog LWC sampled using an active string-fog collector (Usui Kogyo Co., Japan) with two rows of 0.4 mm diameter Teflon strands [Aikawa *et al.*, 2001, 2007] based on the similar concept of Caltech Active Strand Cloudwater Collector near the Rokko Visitor Center (Figure 1b) located at an altitude of 800 m was used in the study. Details of the sampling method and the composition of the collector are described by Aikawa *et al.* [2005].

[24] Hourly meteorological data on wind speed and direction (Ogasawara Keiki Co.LTD., C-W154), air temperature (Ogasawara Keiki Co.LTD., C-T502) and rainfall were measured at a surface weather station of Japan Meteorological Agency (JMA) at the summit of Mt. Rokko (Figure 1b), which is close to the Rokko Visitor Center. WRF calculations of the wind speed and direction at a height of 10 m, and air temperature at a height of 2 m were

Table 2. Measured (Observed) and WRF Calculated Values of Fog Duration and Averaged Liquid Water Content of Fog (LWC) at Rokko Visitor Center in Japan, and Wind Speed (WS) and Wind Direction (WD), Air Temperature (T), and Specific Humidity (q) at the Summit of Mt. Rokko in Japan of Each Fog Event Identified in Figure 4d^a

Event	Fog Duration (hour)			LWC (g m ⁻³)			WS (m s ⁻¹)		WD (deg)		T (°C)		q (g kg ⁻¹)
	Observed	fog-WRF	org-WRF	Observed	fog-WRF	org-WRF	Observed	fog-WRF	Observed	fog-WRF	Observed	fog-WRF	fog-WRF
1	8	12	13	0.149	0.178	0.288	3.65	6.17	138.5	190.3	21.00	21.24	17.35
2	6	6	8	0.115	0.053	0.130	4.60	7.07	148.1	184.2	21.23	21.19	16.80
3	11	10	10	0.120	0.130	0.189	6.21	7.59	146.3	187.9	20.75	20.96	16.95
4	8	16	17	0.171	0.214	0.358	6.96	8.61	165.9	195.1	20.28	21.14	17.23
5	10	14	15	0.210	0.199	0.337	6.00	7.59	155.1	193.8	20.40	20.97	17.05
6	11	13	14	0.199	0.187	0.312	6.13	8.05	166.2	189.5	20.54	20.67	16.65
Mean	9.0	11.8	12.8	0.161	0.160	0.269	5.59	7.51	153.3	190.1	20.70	21.03	17.00

^aThe ‘org-WRF’ and ‘fog-WRF’ represent the calculations using the original version of WRF that includes fog deposition by equation (3), respectively. Note that there was no available data of specific humidity at Mt. Rokko.

compared with measurements made at the weather station located there.

[25] Calculations of fog deposition using SOLVEG and the simple equation of equation (3) were compared with throughfall measurements under three cedar (*Cryptomeria japonica*) coniferous stands around the Rokko Visitor Center. Since no rainfall was observed using tipping bucket rain gauge (Ota Keiki Co.LTD., No.34-T [RA-1]) at both the summit of Mt. Rokko and the Rokko Visitor Center [Kobayashi *et al.*, 2002] during the period, measured fog deposition was simply determined as throughfall data using one tipping bucket rain gauge with a resolution of 0.5 mm (Ota Keiki Co.LTD., No.34-T [RA-1]) equipped with the logger [Kobayashi *et al.*, 2002].

[26] To estimate the uncertainty of the above throughfall measurements, Kobayashi *et al.* [2002] have collected 81 samples of hourly throughfall amount using the same type of two rain gauges set at an opposite direction under the same forest canopy. The result showed the regression line of throughfall amounts had a slope of 1.022 and an intercept 0.22 with a good correlation ($R = 0.946$). From the relationship, the observational error in throughfall measurements was estimated as 0.2–0.26 mm h⁻¹, corresponding to 11–14 mm multiplied observed fog duration throughout the simulation period (Table 2). The error is, however, considered relatively smaller than the observed total throughfall amount during the simulation period was very large as 68 mm (Figure 5b). Although an error associated with evaporation loss from wetted canopy probably accumulated in the estimation of fog deposition [e.g., Bruijnzeel *et al.*, 2011], this effect is considered not so large in the situation as fog episode continued without long fog-free periods, as discussed by Kobayashi *et al.* [1999].

[27] If drizzle appeared during the sampling period, throughfall data was overestimated due to the mixture of fog and drizzle. This could affect the estimation of fog deposition from throughfall data without exclusion of drizzle mixture [Bruijnzeel *et al.*, 2011]. Unfortunately, no information of drizzle is available at the surface weather station at Mt. Rokko, so there may be an error of fog deposition estimation from the measured throughfall data only.

[28] For comparison of vertical distributions of fog between observations and model calculations, we used additional two data sets of throughfall and LWC collected at different field campaigns along the slopes of Mt. Rokko that have been carried out in the following periods: July 1999 to

June 2001 for throughfall, and October 1997 to October 1998.

[29] Figures 2b and 2c show maps of tree or building height and Digital Elevation Model (DEM) that represents all terrain elements including buildings and vegetation, but did not differentiate between elements, respectively, derived from high-resolution GIS data measured by an airborne laser scanner (LIDAR) (Kokusai Kogyo Co., Japan). As shown in the figures, all cedar trees targeted in this study were located with edge or canopy gaps. ‘Forest edges’ such as escarpments, steep slopes, and canopy gaps are produced by either natural or anthropogenic disturbance, and are likely to receive considerably more nutrient and pollutant deposition than the interior of forests [Weathers *et al.*, 1995]. The influence of forest edges on fog deposition at the Rokko Visitor Center is discussed in section 4.2.

4. Results and Discussion

4.1. Effect of Fog Deposition on Prediction of Liquid Water Content of Fog

[30] Figure 3 provides the spatial distributions of calculated mean horizontal and vertical wind speeds and LWC during the simulation period from 19 to 26 July 1999. Upslope winds stronger than 0.1 m s⁻¹ were simulated on the leeward side of southeastern areas near Osaka Bay (Figure 3a). These southern winds carried humid air over the Osaka Bay to Mt. Rokko (Figure 3a) and caused it to condensate along mountain ridges higher than 400 m in altitude (Figures 3b and 3c). The resultant cloud can be explained by an orographic cloud formation due to the upslope condensation mechanism, similar to the results found in mountain areas of Saudi Arabia [Katata *et al.*, 2010]. Although both fog- and org-WRFs simulated fog formulation along Mt. Rokko, the LWC calculated by WRF that includes fog deposition by equation (3) (Figure 3c) was overall smaller than that using org-WRF (Figure 3b). This can be explained by the higher deposition rate of fog liquid water in fog-WRF than in org-WRF.

[31] Figure 4 gives temporal evolution with time in calculations and observations of hourly wind speed and direction, air temperature, and liquid water content of fog at the summit of Mt. Rokko (Figure 1b). General trends in observations of meteorological variables were reproduced in the simulation using both fog- and org-WRFs. The model may have overestimated true wind speed due to the coarse horizontal grid size of input meteorological re-analysis data from 2.5 degrees. In addition, the grid size of 2 km for domain 4 is still too coarse to

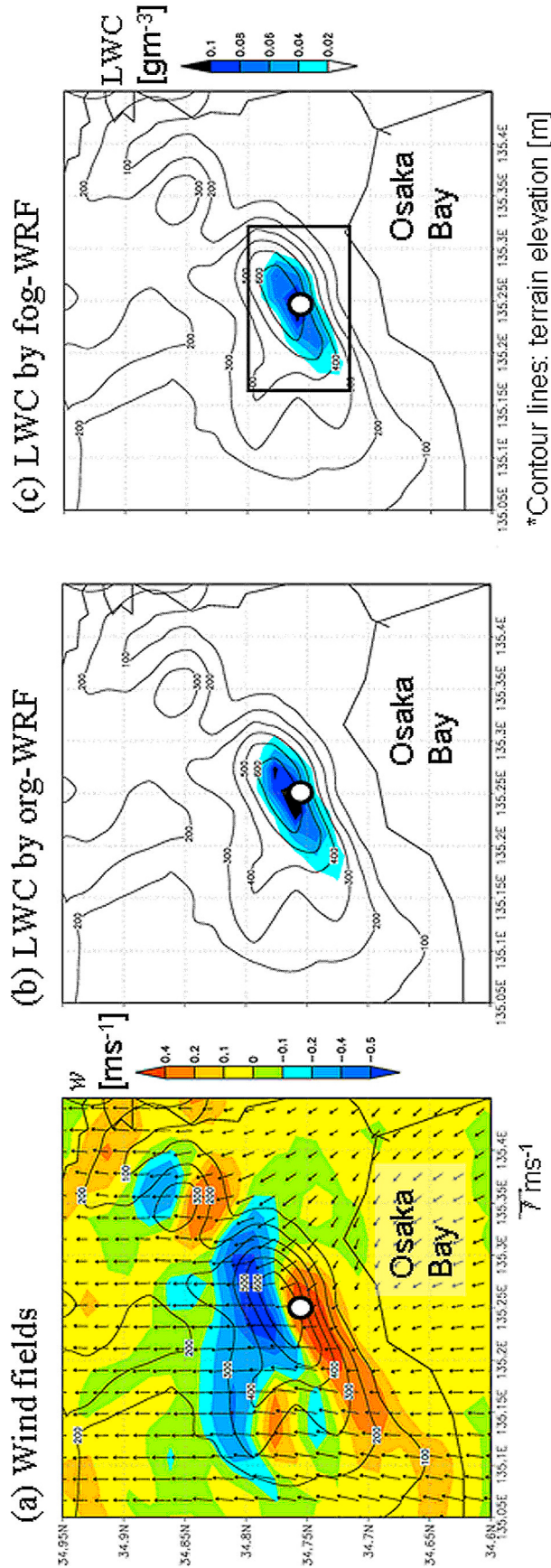


Figure 3. Spatial distributions of mean calculated values from 19 to 26 July 1999 for (a) wind vectors and vertical wind velocity (shaded areas) and (b) fog liquid water content (shaded areas) at the lowest atmospheric layer calculated by the original version of WRF (org-WRF) and (c) that includes fog deposition on forest canopies (fog-WRF). The location of the simulation grid that includes both the Rokko Visitor Center and the summit of Mt. Rokko is plotted in Figures 3b and 3c.

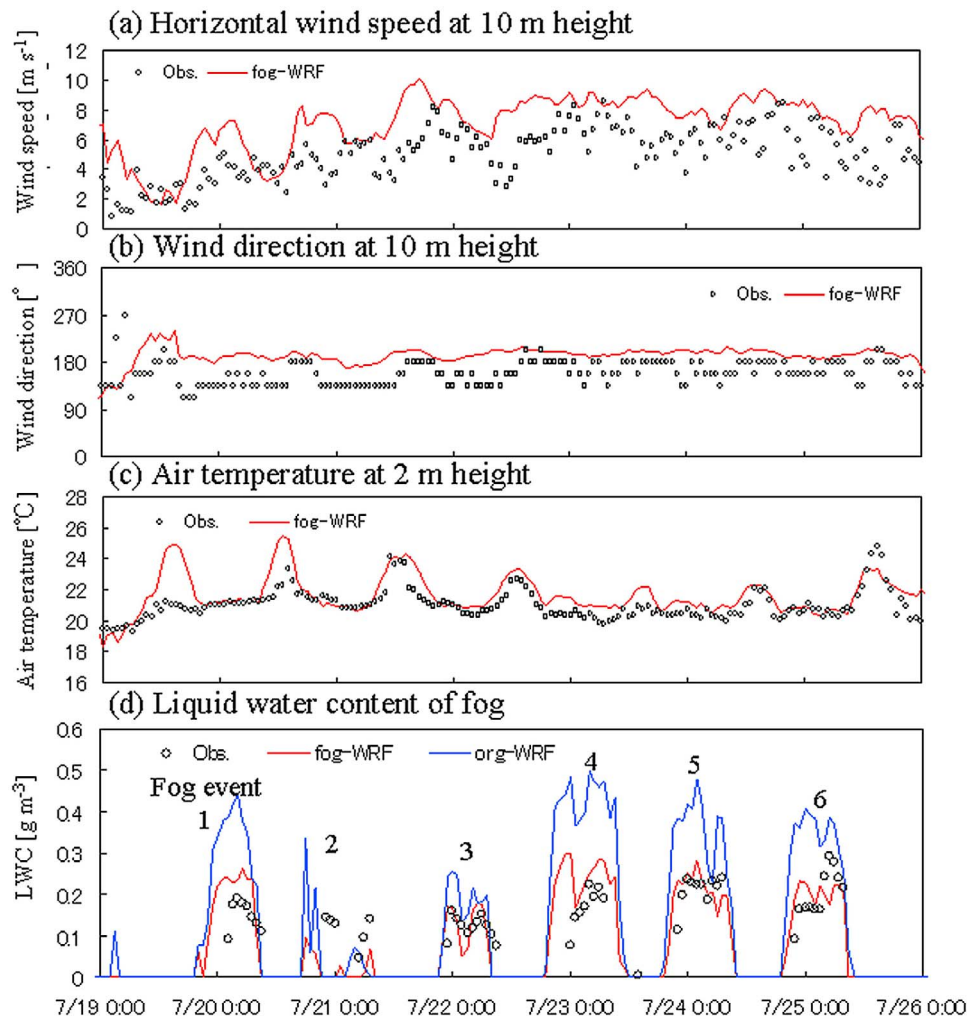


Figure 4. Time series of WRF calculations and measurements (open circles) of hourly (a) horizontal wind speed and (b) direction, (c) air temperature, and (d) liquid water content of fog (LWC) at 35 m height at the summit of Mt. Rokko and Rokko Visitor Center from 19 to 26 July 1999.

resolve the real mountain topography; in fact, the altitude of the grid of domain 4 that includes the summit of Mt. Rokko, for example, was 697.0 m, which is lower than the real altitude of 875.0 m at the summit, as mentioned in section 4.3. Calculated wind speed can be raised by changing the inclination of the mountain slopes. However, characteristic aspects of meteorology, such as southern wind flows from the ocean and low air temperature during fog episodes, were reproduced with only very small errors. It is thus concluded that WRF reproduced basic features in the air temperature and humidity fields during fog episodes on Mt. Rokko.

[32] It can be seen that both fog- and org-WRFs reproduced six fog events, but the LWC calculated by org-WRF was significantly larger than the observations (Figure 4d, blue lines), which is similar to the case of MM5 simulation by Katata *et al.* [2010]. In contrast, fog-WRF successfully simulated LWC for most of fog events at the Rokko Visitor Center (Figure 4d, red lines). This difference between the two calculations is due to the modification of the scheme of fog deposition by equation (3) in fog-WRF. This indicates that fog deposition is crucial for accurate prediction in LWC over mountain forests using the meteorological model.

[33] In the statistics during fog episodes (Table 2), the performance of fog-WRF is apparent in predictions of fog duration and LWC. Mean calculated values in LWC by fog-WRF agreed well with the observations, while org-WRF overestimated it by a maximum of 2.1 times throughout the simulation period. Due to a decrease in LWC by fog deposition, fog duration also decreased in calculations of fog-WRF and was close to observations (Table 2). The results indicate that the effect of fog deposition on fog duration and LWC is significant over forest canopies. Fog deposition onto vegetation should therefore be included in meteorological models to ensure the accurate prediction of cloud and fog episodes over mountainous areas. The simple formula of fog deposition in equation (3) is considered useful for estimating fog deposition onto mountain forests.

[34] As described in section 1, in the mountain forests oriented in a downwind area of industrial and urban cities, such as Mt. Rokko, fog acidification and deposition is highly concerned [e.g., Aikawa *et al.*, 2005]. The meteorological model that includes the simple scheme of fog deposition onto vegetation, fog-WRF, become also an important

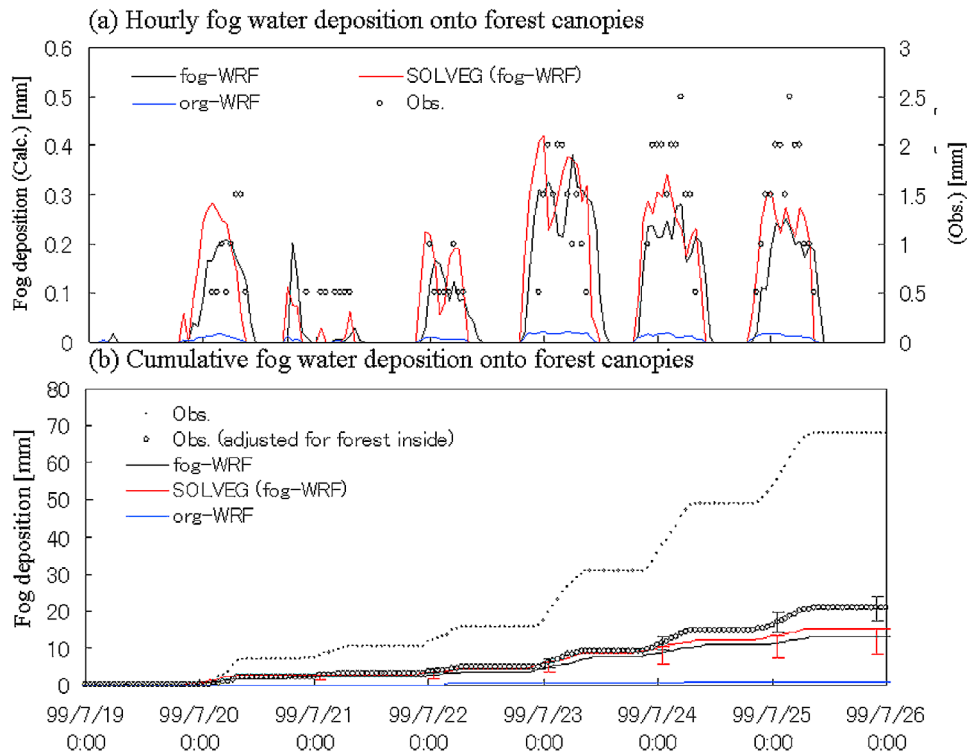


Figure 5. Time series of measurements (solid and open circles) and calculations by the original version of WRF (org-WRF), that includes fog deposition by equation (3) (fog-WRF), and SOLVEG using the outputs from both org- and fog-WRFs of (a) hourly and (b) cumulative fog deposition onto forest canopies at Rokko Visitor Center from 19 to 26 July 1999. Error bars in SOLVEG calculations in Figure 5b show the variances between maximum and minimum values when LAI were set at 3, 4.5, and 6.

tool for estimation of acid fog deposition by coupled with the CTMs [e.g., *Grell et al., 2005; Kajino and Kondo, 2011*].

4.2. Simulation of Fog Deposition Onto Mountainous Forest Canopies

[35] Figure 5 shows the time series of observations and calculations using fog-WRF of hourly and cumulative fog deposition on cedar tree No. 1 (Figure 2b) at the Rokko Visitor Center (Figure 1b). Calculations by org-WRF and SOLVEG using the output from fog-WRFs were also plotted in the figure to confirm the accuracy of a simple linear equation as in equation (3). The trend of observed fog deposition events was generally reproduced by both SOLVEG and fog-WRF, as fog deposition is larger in the last three fog events (No. 4–6) under stronger wind and larger LWC. This indicates that fog-WRF captured the features of fog deposition as being proportional to both wind speed and LWC [*Katata et al., 2008*].

[36] As shown in Figure 5b, the cumulative amount of fog deposition in SOLVEG and fog-WRF was smaller than approximately half of the throughfall observation at the end of the calculations. This may be partially due to an uncertainty in the model settings of the LAI and droplet size of clouds value. From SOLVEG calculations using LAI = 3.0 and 6.0, however, the amount of cumulative fog deposition rather decreased from 15.1 to 8.2 mm at the end of the calculations (Figure 5b, red error bars). With regard to cloud droplet size, its effect on fog deposition was tested using SOLVEG with the mean diameter (D_{mean}) of 5 and 20 μm , and changed the fog deposition amount at the end of the calculations 3.9 mm

increase and 2.7 mm decrease, respectively. However, the large difference between calculations and observations could not be explained by only both effects of LAI and droplet size distribution.

[37] This discrepancy is probably explained by the ‘edge effect’, the phenomenon whereby deposition to forest edges increases strongly compared to that inside the forest stand due to inflow and advection processes [*Hasselrot and Grennfelt, 1987; Beier et al., 1992; Draaijers et al., 1994; Weathers et al., 2001; Wuyts et al., 2008*]. Clouds travel a long distance along the mountain ridge that consists of mainly closed forest canopies, so LWC data is considered to show representative values over the closed forest. In contrast, throughfall measurements strongly depend on the heterogeneous structure of forests such as edges or gaps. The distance of edge is one of the crucial parameter that can cause a large variation in throughfall amount as shown in the above literature. In fact, Cedar tree No. 1 was located at the edge of the forest directly facing the upstream wind from a southerly direction (Figure 2c), and was considerably affected by the edge effect. This assumption is considered reasonable because, in fact, the other cedar trees (No. 2 and 3) positioned inside the forest (Figure 2c) had less fog deposition, only 54 and 86% of that of No. 1, respectively, based on throughfall measurements from October 1997 to 1998 [*Kobayashi et al., 1999*]. The edge effect cannot be taken into account into fog-WRF and SOLVEG since they are one-dimensional vertical models.

[38] To compare the calculations by models with the observations of fog deposition inside the mountain forest,

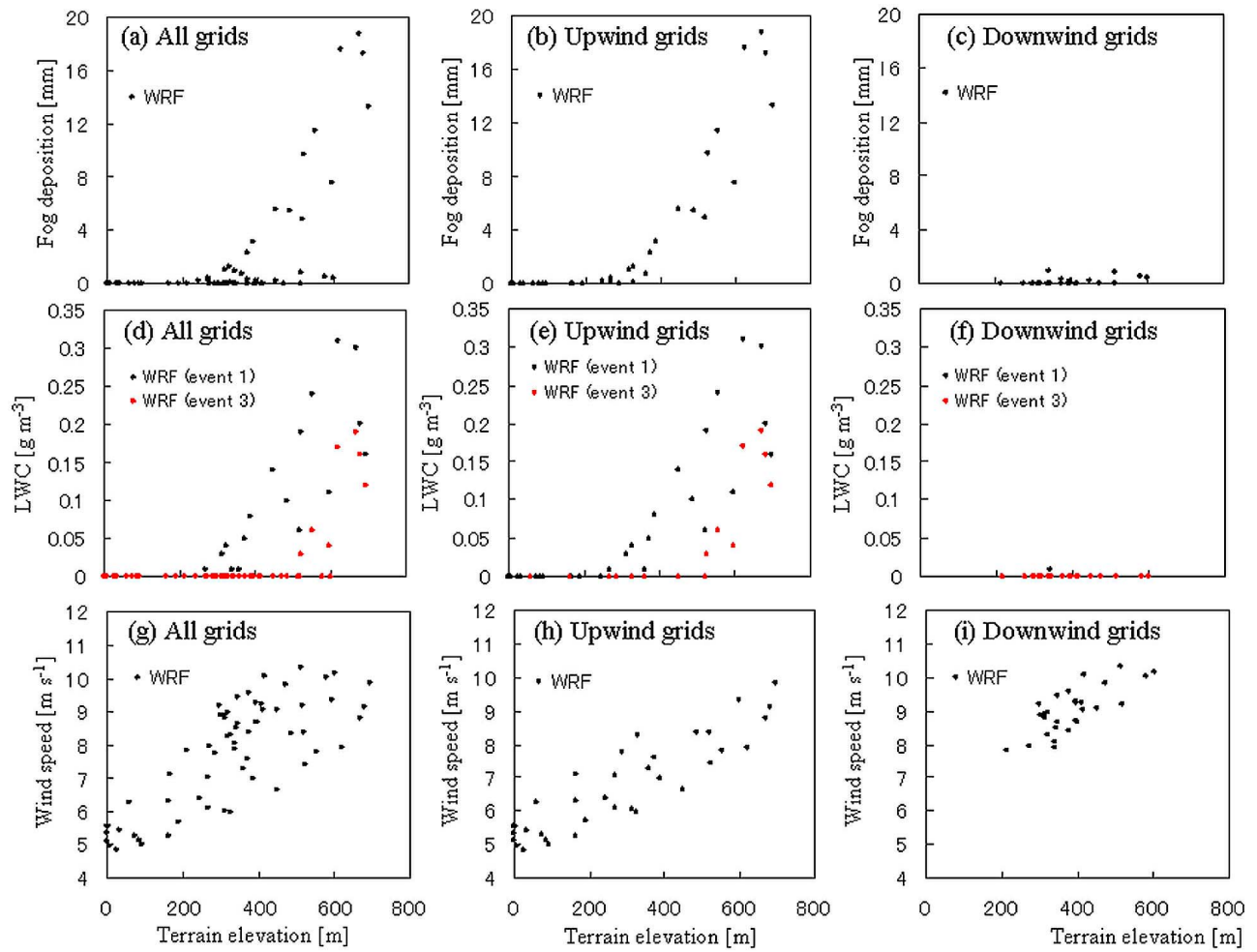


Figure 6. Calculations of (a–c) cumulative fog deposition onto forest canopies throughout the simulation period, (d–f) liquid water content of fog (LWC) for the fog events No. 1 and 3 defined in Figure 4d, and (g–i) averaged wind speed at 35 m in height calculated by WRF that includes fog deposition by equation (3) (fog-WRF) plotted against terrain elevation for all, upwind, and downwind simulation grids of Mt. Rokko region (square in Figure 3c).

the authors estimated fog deposition inside the forest using the enhancement factor due to the edge effect proposed by Draaijers *et al.* [1994]. Draaijers *et al.* [1994] showed that net throughfall flux, Th_{eg} , decreases as an exponential decay function of the distance to the forest edge, x [m], divided by the edge (canopy) height, h :

$$Th_{eg} = Th_0 \exp(-x/h) + Th_{int}, \quad (4)$$

where Th_0 and Th_{int} are the net throughfall flux at the forest edge ($x/h = 0$) and inside the forest, respectively. They concluded that, throughfall flux at the very edge of the forest (Th_0) was determined as approximately 4 times larger than that inside the forest (Th_{int}) for coarse-mode (super-micron) particles, such as Na^+ , Cl^- and Mg^{2+} .

[39] Since the particle radius in coarse-mode is of the same order in fog droplet, the throughfall enhancement factor at the very edge, i.e., Th_0/Th_{int} can be assumed to be 4. Here, by taking into account $x/h = 0.31$ – 0.77 derived from observed canopy height ($h = 13$ m) for cedar tree No. 1 and $x = 4$ – 10 m from Figure 2c, the Th_{eg}/Th_0 was estimated as

2.85–3.93 using equation (4). Dividing observed throughfall data by these values of 2.85 and 3.93 (Figure 5b, open circles) to exclude the edge effect, calculations of fog deposition by fog-WRF (13.1 mm) agreed reasonably well with the observations (17.3–23.8 mm) as well as the calculations SOLVEG using LWC output from fog-WRF (15.2 mm) at the end of the calculation period. The results show that equation (3) incorporated in fog-WRF has good performance in predicting fog deposition onto cedar trees at the Rokko Visitor Center.

[40] By contrast, cumulative fog deposition calculated by org-WRF (0.85 mm) was clearly smaller than observations (Figure 5b, green lines). The difference between org-WRF and fog-WRF in predicting fog deposition is due to the fact that the exchange coefficient calculated by org-WRF ($c_h |u| = 0.008$ – 0.05 m s⁻¹) is smaller than the deposition velocity of fog ($V_d = 0.065$ – 0.37 m s⁻¹), as mentioned in section 2.2. The conclusion is therefore drawn that a meteorological model that includes equation (3) can be used to estimate fog deposition in mountain forests in East Asia.

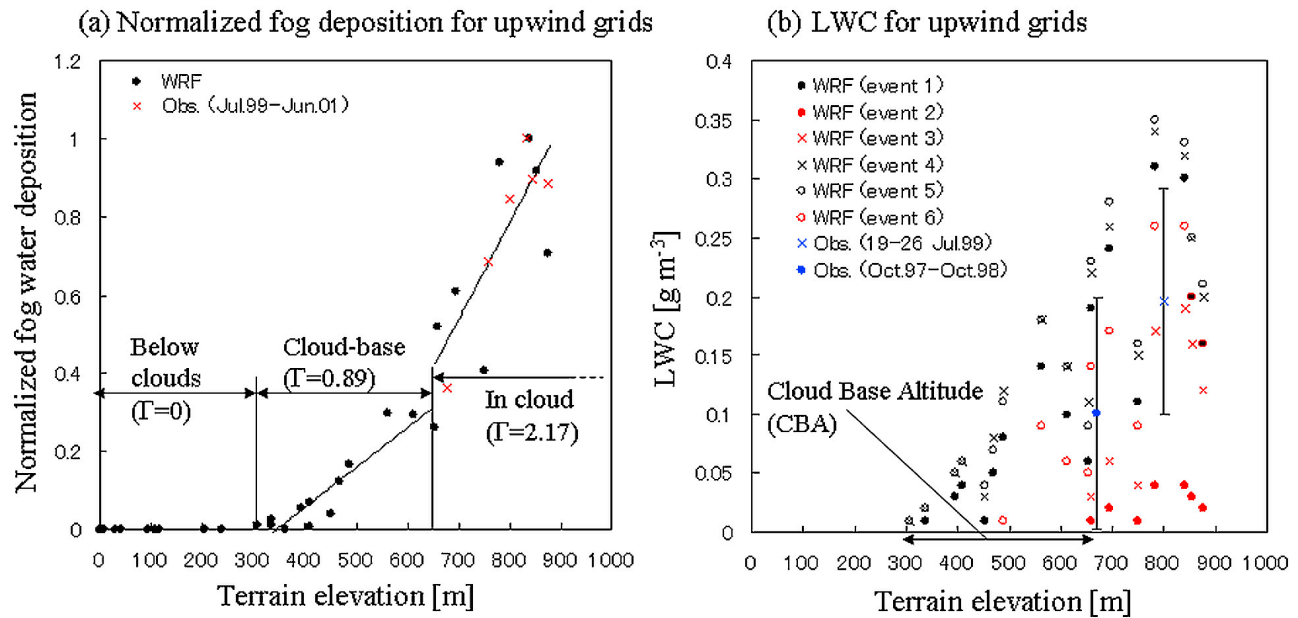


Figure 7. Calculations by WRF that includes fog deposition by equation (3) (fog-WRF) of (a) normalized cumulative fog deposition onto forest canopies throughout the simulation period and (b) mean liquid water content of fog (LWC) for fog events with high (black symbols) and low LWC (red symbols) plotted against terrain elevation for the upwind simulation grids of Mt. Rokko region (square in Figure 3c). The Γ in Figure 7a is the increase rate of normalized fog deposition with normalized terrain height. The data of throughfall observations by Kobayashi and Nakagawa [2002] and LWC by Kobayashi *et al.* [1999] are also plotted in Figures 7a and 7b, respectively.

[41] Note that fog deposition can affect the water, heat and even CO_2 exchanges that take place between the atmosphere and forest canopies [Katata *et al.*, 2010], causing changes in the atmospheric field (e.g., air temperature and humidity, and CO_2 concentration) over forest canopies. Equation (3) only calculates the amount of fog deposition and does not include such complicated exchange processes between atmosphere and vegetation. Further research using the meteorological model coupled with a detailed land surface model such as SOLVEG is thus required to reveal the feedback of fog deposition to the atmosphere.

4.3. Altitude Dependence of Fog Deposition in Mountain Forests

[42] The horizontal distribution of fog deposition onto forest canopies in all simulation grids involved in the region around Mt. Rokko (135.14°E–135.32°E in longitude and 34.7°N–34.82°N in latitude, shown as the square in Figure 3c) was investigated from calculations using fog-WRF. Figure 6 shows the altitude dependency of calculated cumulative fog deposition, LWC and horizontal wind speed for all simulation grids in the above region. To characterize fog deposition in the study area, the Mt. Rokko region was divided into two parts, namely upwind (NE direction) and downwind (SW direction) from the mountain ridge. In Figures 6a and 6b, there was in general greater fog deposition with increasing terrain elevation. Fog deposition was, however, approximately zero at almost all ‘downwind’ grids (Figure 6c) due to the lack of fog or clouds (Figure 6f). This provides evidence that simulated fog or clouds on Mt. Rokko were completely based on orographical uplifting from the lowland area. In contrast, it can be seen that the calculated LWC increased with an increase in elevation as

well as fog deposition for ‘upwind’ grids (Figure 6e). In the ‘upwind’ grids facing southeastern mountain slopes, both fog deposition and LWC increased drastically above approximately 300 m in height (Figures 6b and 6e). This suggests that the cloud base altitude (CBA), which can be determined as the elevation where $\text{LWC} > 0.017 \text{ g m}^{-3}$ (i.e., foggy condition), was approximately 300 m.

[43] Comparing the LWC in two fog events (No. 1 and No. 3), however, there was a large discrepancy in CBA between the two. This difference could be explained by the difference in mainly air temperature among the fog events. When plotting calculations of specific humidity against air temperature for all fog events from Table 2 (not shown) except for event No. 2 that clouds not continuously but intermittently covered over the Rokko Visitor Center, specific humidity clearly increased with an increase of air temperature during the simulation period. In the cloud microphysics scheme in the WRF model, super-saturation in clouds mainly depends on air temperature if effects of condensation, entrainment, and adiabatic ascent of air parcel etc. are assumed to be neglected. Thus, the difference in air temperature can be the reason that the lower CBA value for event No. 1 ($\cong 250 \text{ m}$) than that for No. 3 ($\cong 500 \text{ m}$) (Figure 6e) appeared in the simulation result.

[44] To investigate the relationship between CBA and fog deposition, cumulative fog deposition (normalized using fog-WRF output from the grid that includes the summit of Mt. Rokko) and LWC for all fog events compared for ‘upwind’ grids were plotted against the terrain elevation (Figure 7). To compare the observational data from Mt. Rokko, all terrain elevations in domain 4 of fog-WRF were adjusted to reflect the ratio of the maximum elevation at the grid of domain 4 (697.0 m) to the true elevation at the summit (875.0 m). This is

because, as mentioned in section 4.1, the spatial resolution of 2 km in domain 4 could not completely describe the mountainous terrain. For comparison between calculations and observations, we also plotted data collected at a later campaign of throughfall measurements (July 1999 to June 2001) in Figure 7a. Above 655 m in altitude, the calculations of normalized fog deposition agreed with the observations derived from annual mean throughfall data collected along the slopes of Mt. Rokko from July 1999 to June 2001 [Kobayashi and Nakagawa, 2002] (Figure 7a). It can also be seen that the calculations of LWC at an altitude of 800 m were larger than those at 670 m, which agreed with the observations from Figures 6d and 6e and annual mean values collected at an earlier campaign from October 1997 to October 1998 [Kobayashi et al., 1999] (Figure 7b).

[45] From Figure 7a, it can be seen that the rate of increase in fog deposition with normalized terrain height, Γ , was smaller when below 300 m than when above 655 m in altitude. Based on equation (2), in which $c_h |\mathbf{u}|$ was replaced with V_d by equation (3), the fog deposition flux F_{qc} can be determined by LWC and horizontal wind speed with the use of the same vegetation parameters. Because mean horizontal wind speed increased with altitude at almost the same rate in all elevation ranges (Figure 6h), LWC due to a change in CBA determined the slope Γ in the case of the Mt. Rokko region. Since the minimum value of CBA was 300 m in altitude in the simulation period (Figure 7b), clouds did not cover the areas < 300 m altitude and thus $\Gamma = 0$ (Figure 7a) there, while $\Gamma = 2.17$ at the highland > 655 m in elevation where was always above CBA. The elevation range between 300 and 600 m is transition region for CBA, which has the lower values of $\Gamma = 0.89$ (Figure 7a) than that above 655 m. From the above discussion, fog deposition in the Mt. Rokko region can be characterized as comprising the following three regions: (1) ‘Below clouds’: no fog deposition because the altitude is always below CBA (0–300 m in elevation); (2) ‘Cloud base’: fog is frequently but not always deposited, depending on CBA (300–655 m in elevation); (3) ‘In cloud’: fog is always deposited because the altitude is always above CBA (>655 m in elevation).

[46] In addition, if the cloud top is below the summit of the mountains, the following fourth region could be defined: (4) ‘Above cloud’: no cloud covers the region because its elevation is above the cloud deck (this is not the case for Mt. Rokko).

[47] In the fourth region, it is expected that fog deposition amount becomes the highest at the uppermost part of the cloud and then gradually declines toward the mountain top because the region is not covered with clouds. Since the fourth region did not appear in the case of Mt. Rokko, we focus on the first three regions below.

[48] Since the cloud deck size is the important scaling parameter for the above four regions, normalized fog deposition using that at the top of cloud deck, f_{fg} , in the Mt. Rokko region can be determined from fog-WRF calculations under the following fitting equations:

$$\bar{C}_{fg} = C_{fg}/C_{fgtop} = \begin{cases} 0 & 0\text{ m} < z < 300\text{ m} \\ 2.17(z/H) - 1.2 & 300\text{ m} \leq z < 655\text{ m}, \\ 0.89(z/H) - 0.35 & 655\text{ m} \leq z \leq H \end{cases} \quad (5)$$

where C_{fg} and C_{fgtop} [mm] are the cumulative fog deposition at a certain elevation and at the top of cloud deck (that corresponds to the summit of mountains in the case of Mt. Rokko), respectively, z the terrain elevation [m], and H the altitude of the top of cloud deck [m]. As mentioned above, it is clear that Γ for the ‘in cloud’ region (= 2.17) was higher than that for the ‘cloud base’ region (= 0.89), since the variation in CBA reduced the fog frequency, LWC and fog deposition in the latter region. The simple linear formulation of equation (5) using Γ is considered valid for mountain forests such as those on Mt. Rokko, where forest canopies are distributed homogeneously with changing altitude. Thus, if the data for C_{fg} are available at a certain altitude (z) and the Γ is determined by the meteorological simulation at a target mountain forest, C_{fgtop} can be determined by equation (5) and as a result, the vertical distribution of fog deposition can be roughly estimated in a mountain forest. Equation (5) has only one parameter Γ which can be numerically determined, so this is useful to estimate the vertical distribution of fog deposition when a number of throughfall data are unavailable at a target mountain forest. Meanwhile, the forest structure (e.g., small tree density and large gaps, considerably affected by ‘edge effect’ discussed in section 4.2) in some other cloud forests may not be as spatially homogeneous as the forest canopies on Mt. Rokko. In this case, the relationship between fog deposition and altitude may not be as simple as equation (5). To investigate the applicability of equation (5), therefore, long-term (seasonal, annual or interannual) simulations of fog deposition using fog-WRF should be employed for various mountain cloud forests throughout the world.

5. Conclusion

[49] The scheme of fog deposition onto vegetation was incorporated into a meteorological model for studies of fog occurrence, acidification, and deposition in mountain forests. The meteorological model (WRF) was modified to calculate the removal of cloud liquid water due to fog deposition using the simple linear function of fog deposition onto vegetation [Katata et al., 2008]. A modified version of WRF including fog deposition (fog-WRF) was tested in forests on Mt. Rokko in Japan. Since the simple linear function of fog deposition has been parameterized in German coniferous forests, simulations using a detailed multi-layer fog deposition model (SOLVEG) were also carried out to confirm the performance of fog-WRF under climatic conditions in East Asia. By taking into account the process of fog deposition, fog-WRF provided a clearly better prediction of the liquid water content of fog (LWC) than the original version of WRF (org-WRF). As well as the SOLVEG calculations, fog-WRF reproduced fog deposition inside forests on Mt. Rokko calculated from throughfall observations after excluding increased fog deposition at the forest edges.

[50] In the analyses of vertical distributions of LWC and fog deposition calculated by fog-WRF, fog deposition in the region of Mt. Rokko can be characterized as the linear relationship between normalized fog deposition and elevation for the four regions of ‘below clouds’, ‘cloud base’, ‘in cloud’, and ‘above cloud’. Using the linear equation and data from throughfall observations at given altitude, the vertical distribution of fog deposition in mountain forests

can be roughly estimated. The relationship between fog deposition and altitude should be confirmed by long-term simulations of fog deposition using fog-WRF in various mountain cloud forests that have the different forest structures in future. A meteorological model that includes a simple linear equation of fog deposition can provide mapping for the distribution of fog deposition onto forest canopies in mountain cloud forests.

[51] **Acknowledgments.** The authors wish to express their gratitude to H. Ueda, M. Igawa, H. Okouchi, N. Takenaka, and M. Uematsu for helpful comments and discussion on the calculation results. The present study was partially supported by a Grant-in-Aid for Scientific Research on Innovative Areas (21120512) and for Young Scientists B (21710035) from the Ministry of Education, Culture, Sports, Science and Technology. The data sets used for this study were provided from a cooperative research project JRA-25 long-term reanalysis by the Japan Meteorological Agency (JMA) and the Central Research Institute of Electric Power Industry (CRIEPI).

References

- Aikawa, M., T. Hiraki, M. Shoga, and M. Tamaki (2001), Fog and precipitation chemistry at Mt. Rokko in Kobe, April 1997–March 1998, *Water Air Soil Pollut.*, *130*, 1517–1522, doi:10.1023/A:1013945905410.
- Aikawa, M., T. Hiraki, M. Shoga, and M. Tamaki (2005), Chemistry of fog water collected in the Mt. Rokko area (Kobe City, Japan) between April 1997 and March 2001, *Water Air Soil Pollut.*, *160*, 373–393, doi:10.1007/s11270-005-3117-1.
- Aikawa, M., T. Hiraki, M. Suzuki, M. Tamaki, and M. Kasahara (2007), Separate chemical characterizations of fog water, aerosol, and gas before, during, and after fog events near an industrialized area in Japan, *Atmos. Environ.*, *41*, 1950–1959, doi:10.1016/j.atmosenv.2006.10.049.
- Alewell, C., B. Manderscheid, H. Meesenburg, and J. Bittersohl (2000), Environmental chemistry – Is acidification still an ecological threat?, *Nature*, *407*, 856–857, doi:10.1038/35038158.
- Beier, C., P. Gundersen, and L. Rasmussen (1992), A new method for estimation of dry deposition of particles based on throughfall measurements in a forest edge, *Atmos. Environ., Part A*, *26*, 1553–1559.
- Bruijnzeel, L. A., M. Mulligan, and F. N. Scatena (2011), Hydrometeorology of tropical montane cloud forests: Emerging patterns, *Hydrol. Processes*, *25*, 465–498, doi:10.1002/hyp.7974.
- Chen, F., and J. Dudhia (2001), Coupling an advanced land-surface/hydrology model with the Penn State/NCAR MM5 modeling system. Part I: Model description and implementation, *Mon. Weather Rev.*, *129*, 569–585, doi:10.1175/1520-0493(2001)129<0569:CAALSH>2.0.CO;2.
- Choullart, T. W., et al. (1997), The Great Dun Fell Cloud Experiment 1993: An overview, *Atmos. Environ.*, *31*, 2393–2405, doi:10.1016/S1352-2310(96)00316-0.
- Collatz, G. J., J. T. Ball, C. Grivet, and J. A. Berry (1991), Physiological and environmental regulation of stomatal conductance, photosynthesis and transpiration: A model that includes a laminar boundary layer, *Agric. For. Meteorol.*, *54*, 107–136, doi:10.1016/0168-1923(91)90002-8.
- Collatz, G. J., M. Ribas-Carbo, and J. A. Berry (1992), Coupled photosynthesis-stomatal conductance model for leaves of C4 plants, *Aust. J. Plant Physiol.*, *19*, 519–538, doi:10.1071/PP9920519.
- Conley, D. J., H. W. Paerl, R. W. Howarth, D. F. Boesch, S. P. Seitzinger, K. E. Havens, C. Lancelot, and G. E. Likens (2009), Controlling eutrophication: Nitrogen and phosphorus, *Science*, *323*, 1014–1015, doi:10.1126/science.1167755.
- Crow, P. (2005), The influence of soils and species on tree root depth, *FCIN078*, pp. 1–8, Environ. and Human Sci. Div., For. Comm., Farnham, U. K.
- Deirmendjian, D. (1969), *Electromagnetic Scattering on Spherical Polydispersions*, 290 pp., Elsevier, New York.
- Draaijers, G. P. J., R. Van Ek, and W. Bleuten (1994), Atmospheric deposition in complex forest landscapes, *Boundary Layer Meteorol.*, *69*, 343–366, doi:10.1007/BF00718124.
- Dudhia, J. (1989), Numerical study of convection observed during the winter monsoon experiment using a mesoscale two-dimensional model, *J. Atmos. Sci.*, *46*, 3077–3107, doi:10.1175/1520-0469(1989)046<3077:NSOCOD>2.0.CO;2.
- Erisman, J. W. (1994), Evaluation of a surface resistance parametrization of sulphur dioxide, *Atmos. Environ.*, *28*, 2583–2594, doi:10.1016/1352-2310(94)90432-4.
- Erisman, J. W., G. Draaijers, J. Duyzer, P. Hofschröder, N. Van Leeuwen, F. Römer, W. Ruijgrok, P. Wyers, and M. Gallagher (1997), Particle deposition to forests—Summary of results and application, *Atmos. Environ.*, *31*, 321–332, doi:10.1016/S1352-2310(96)00223-3.
- Erisman, J. W., M. G. Mennen, D. Fowler, C. R. Flechard, G. Spindler, A. Grüner, J. H. Duyzer, W. Ruijgrok, and G. P. Wyers (1998), Deposition monitoring in Europe, *Environ. Monit. Assess.*, *53*, 279–295, doi:10.1023/A:1005818820053.
- Farquhar, G. D., P. M. Firth, R. Wetselaar, and B. Weir (1980), On the gaseous exchange of ammonia between leaves and the environment: Determination of the ammonia compensation point, *Plant Physiol.*, *66*, 710–714, doi:10.1104/pp.66.4.710.
- Grell, G. A., S. E. Peckham, R. Schmitz, S. A. McKeen, G. Frost, W. C. Skamarock, and B. Eder (2005), Fully coupled “online” chemistry within the WRF model, *Atmos. Environ.*, *39*, 6957–6975, doi:10.1016/j.atmosenv.2005.04.027.
- Hasselrot, B., and P. Grennfelt (1987), Deposition of air pollutants in a wind-exposed forest edge, *Water Air Soil Pollut.*, *34*, 135–143, doi:10.1007/BF00184756.
- Herckes, P., R. Wendling, N. Sauret, P. Mirabel, and H. Wortham (2002), Cloudwater studies at a high elevation site in the Vosges Mountains (France), *Environ. Pollut.*, *117*, 169–177, doi:10.1016/S0269-7491(01)00139-7.
- Hicks, B., R. Hosker, T. Meyers, and J. Womack (1991), Dry deposition inferential measurement techniques—I. Design and tests of a prototype meteorological and chemical system for determining dry deposition, *Atmos. Environ., Part A*, *25*, 2345–2359.
- Hong, S.-Y., and J.-O. J. Lim (2006), The WRF single-moment 6-class microphysics scheme (WSM6), *J. Korean Meteorol. Soc.*, *42*, 129–151.
- Igawa, M., K. Matsumura, and H. Okochi (2002), High frequency and large deposition of acid fog on high elevation forest, *Environ. Sci. Technol.*, *36*, 1–6, doi:10.1021/es0105358.
- Janjic, Z. I. (1994), The step-mountain eta coordinate model: Further developments of the convection, viscous sublayer and turbulence closure schemes, *Mon. Weather Rev.*, *122*, 927–945, doi:10.1175/1520-0493(1994)122<0927:TSMECM>2.0.CO;2.
- Janjic, Z. I. (2000), Comments on “Development and evaluation of a convection scheme for use in climate models,” *J. Atmos. Sci.*, *57*, 3686, doi:10.1175/1520-0469(2000)057<3686:CODAEO>2.0.CO;2.
- Janjic, Z. I. (2002), Nonsingular implementation of the Mellor–Yamada Level 2.5 scheme in the NCEP Meso model, *NCEP Off. Note 437*, 61 pp., Natl. Cent. for Environ. Predict., Camp Springs, Md.
- Kajino, M., and Y. Kondo (2011), EMTACS: Development and regional-scale simulation of a size, chemical, mixing type and soot shape resolved atmospheric particle model, *J. Geophys. Res.*, *116*, D02303, doi:10.1029/2010JD015030.
- Katata, G., H. Nagai, H. Ueda, N. Agam, and P. R. Berliner (2007), Development of a land surface model including evaporation and adsorption processes in the soil for the land-air exchange in arid regions, *J. Hydrometeorol.*, *8*, 1307–1324, doi:10.1175/2007JHM829.1.
- Katata, G., H. Nagai, T. Wrzesinsky, O. Klemm, W. Eugster, and R. Burkard (2008), Development of a land surface model including cloud water deposition on vegetation, *J. Appl. Meteorol. Climatol.*, *47*, 2129–2146, doi:10.1175/2008JAMC1758.1.
- Katata, G., H. Nagai, M. Kajino, H. Ueda, and Y. Hozumi (2010), Numerical study of fog deposition on vegetation for atmosphere–land interactions in semi-arid and arid regions, *Agric. For. Meteorol.*, *150*, 340–353, doi:10.1016/j.agrformet.2009.11.016.
- Katata, G., H. Nagai, L. Zhang, A. Held, D. Serça, and O. Klemm (2011), Development of an atmosphere-soil-vegetation model for investigation of radioactive materials transport in the terrestrial biosphere, *Prog. Nucl. Sci. Technol.*, in press.
- Klemm, O., and T. Wrzesinsky (2007), Fog deposition fluxes of water and ions to a mountainous site in Central Europe, *Tellus, Ser. B*, *59*, 705–714, doi:10.1111/j.1600-0889.2007.00287.x.
- Klemm, O., T. Wrzesinsky, and C. Scheer (2005), Fog water flux at a canopy top: Direct measurement versus one-dimensional model, *Atmos. Environ.*, *39*, 5375–5386.
- Kobayashi, T., and Y. Nakagawa (2002), Spacial distribution of cloud water deposition and acid deposition to the canopies of *Cryptomeria Japonica* at the ridge of Mt. Rokko (in Japanese with English abstract, figures, and tables), *Rep. Environ. Sci. Inst. Hyogo Pref.*, *33*, 73–78.
- Kobayashi, T., Y. Nakagawa, M. Tamaki, T. Hiraki, M. Aikawa, and M. Shoga (1999), Estimation of acid deposition to forest canopies via cloud water by means of throughfall measurements and cloud water collection—Measurements in *Cryptomeria Japonica* stands at Mt. Rokko (in Japanese with English abstract, figures, and tables), *Environ. Sci.*, *12*, 399–411.
- Kobayashi, T., Y. Nakagawa, M. Tamaki, T. Hiraki, and M. Aikawa (2002), Temporal variation of cloud water deposition to *Cryptomeria Japonica*—Fog drip observed in the coniferous forest stands at Mt. Rokko in Kobe (in Japanese with English abstract, figures, and tables), *Environ. Sci.*, *15*, 151–161.

- Kondo, J., and T. Watanabe (1992), Studies on the bulk transfer coefficients over a vegetated surface with a multilayer energy budget model, *J. Atmos. Sci.*, *49*, 2183–2199, doi:10.1175/1520-0469(1992)049<2183:SOTBTC>2.0.CO;2.
- Kunkel, B. A. (1984), Parameterization of droplet terminal velocity and extinction coefficient in fog models, *J. Appl. Meteorol.*, *23*, 34–41, doi:10.1175/1520-0450(1984)023<0034:PODTVA>2.0.CO;2.
- Lange, C. A., J. Matschullat, F. Zimmermann, G. Sterzik, and O. Wienhaus (2003), Fog frequency and chemical composition of fog water—A relevant contribution to atmospheric deposition in the eastern Erzgebirge, Germany, *Atmos. Environ.*, *37*, 3731–3739, doi:10.1016/S1352-2310(03)00350-9.
- Lovett, G. M. (1984), Rates and mechanisms of cloud water deposition to a subalpine balsam fir forest, *Atmos. Environ.*, *18*, 361–371, doi:10.1016/0004-6981(84)90110-0.
- Lovett, G. M., and J. D. Kinsman (1990), Atmospheric pollutant deposition to high-elevation ecosystems, *Atmos. Environ., Part A*, *24*, 2767–2786.
- Meyers, T. P., P. Finkelstein, J. Clarke, T. G. Ellestad, and P. F. Sims (1998), A multilayer model for inferring dry deposition using standard meteorological measurements, *J. Geophys. Res.*, *103*, 22,645–22,661, doi:10.1029/98JD01564.
- Mlawer, E. J., S. J. Taubman, P. D. Brown, M. J. Iacono, and S. A. Clough (1997), Radiative transfer for inhomogeneous atmosphere, RRTM, a validated correlated-k model for the long wave, *J. Geophys. Res.*, *102*, 16,663–16,682, doi:10.1029/97JD00237.
- Nagai, H. (2002), Validation and sensitivity analysis of a new atmosphere-soil-vegetation model, *J. Appl. Meteorol.*, *41*, 160–176, doi:10.1175/1520-0450(2002)041<0160:VASAOA>2.0.CO;2.
- Nagai, H. (2003), Validation and sensitivity analysis of a new atmosphere-soil-vegetation model. Part II: Impacts on in-canopy latent heat flux over a winter wheat field determined by detailed calculation of canopy radiation transmission and stomatal resistance, *J. Appl. Meteorol.*, *42*, 434–451, doi:10.1175/1520-0450(2003)042<0434:VASAOA>2.0.CO;2.
- Nagai, H. (2005), Incorporation of CO₂ exchange processes into a multilayer atmosphere-soil-vegetation model, *J. Appl. Meteorol.*, *44*, 1574–1592, doi:10.1175/JAM2293.1.
- Nakanishi, M., and H. Niino (2004), An improved Mellor–Yamada level-3 model with condensation physics: Its design and verification, *Boundary Layer Meteorol.*, *112*, 1–31, doi:10.1023/B:BOUN.0000020164.04146.98.
- Pleim, J. E., A. Xiu, P. L. Finkelstein, and T. L. Otte (2001), A coupled land-surface and dry deposition model and comparison to field measurements of surface heat, moisture, and ozone fluxes, *Water Air Soil Pollut. Focus*, *1*, 243–252, doi:10.1023/A:1013123725860.
- Shimadera, H., A. Kondo, A. Kaga, K. L. Shrestha, and Y. Inoue (2009), Contribution of transboundary air pollution to ionic concentrations in fog in the Kinki Region of Japan, *Atmos. Environ.*, *43*, 5894–5907, doi:10.1016/j.atmosenv.2009.08.022.
- Skamarock, W. C., J. B. Klemp, J. Dudhia, D. O. Gill, D. M. Barker, M. G. Duda, X. Y. Huang, W. Wang, and J. G. Powers (2008), A description of the Advanced Research WRF Version 3, *NCAR Tech. Note NCAR/TN-475+STR*, 125 pp., Natl. Cent. for Atmos. Res., Boulder, Colo.
- Slinn, W. G. N. (1982), Predictions for particle deposition to vegetative canopies, *Atmos. Environ.*, *16*, 1785–1794, doi:10.1016/0004-6981(82)90271-2.
- Weathers, K. C., G. M. Lovett, and G. E. Likens (1995), Cloud deposition to a spruce forest edge, *Atmos. Environ.*, *29*, 665–672, doi:10.1016/1352-2310(94)00317-E.
- Weathers, K. C., M. L. Cadenasso, and S. T. A. Pickett (2001), Forest edges as nutrient and pollutant concentrators: Potential synergisms between fragmentation, forest canopies, and the atmosphere, *Conserv. Biol.*, *15*, 1506–1514, doi:10.1046/j.1523-1739.2001.01090.x.
- Wesely, M. L. (1989), Parameterization of surface resistances to gaseous dry deposition in regional-scale numerical models, *Atmos. Environ.*, *23*, 1293–1304, doi:10.1016/0004-6981(89)90153-4.
- Wesely, M. L., and B. B. Hicks (2000), A review of the current status of knowledge on dry deposition, *Atmos. Environ.*, *34*, 2261–2282, doi:10.1016/S1352-2310(99)00467-7.
- Wu, Y., B. Brashers, P. L. Finkelstein, and J. E. Pleim (2003), A multilayer biochemical dry deposition model. 1. Model formulation, *J. Geophys. Res.*, *108*(D1), 4013, doi:10.1029/2002JD002293.
- Wuyts, K., A. De Schrijver, J. Staelens, M. Gielis, G. Geudens, and K. Veheyen (2008), Patterns of throughfall deposition along a transect in forest edges of silver birch and Corsican pine, *Can. J. For. Res.*, *38*, 449–461, doi:10.1139/X07-181.
- Zhang, L., S. Gong, J. Padro, and L. Barrie (2001), A size-segregated particle dry deposition scheme for an atmospheric aerosol module, *Atmos. Environ.*, *35*, 549–560, doi:10.1016/S1352-2310(00)00326-5.
- Zhang, L., M. D. Moran, P. A. Makar, J. R. Brook, and S. Gong (2002), Modelling gaseous dry deposition in AURAMS: A unified regional air-quality modelling system, *Atmos. Environ.*, *36*, 537–560, doi:10.1016/S1352-2310(01)00447-2.
- Zhang, L., J. R. Brook, and R. Vet (2003), A revised parameterization for gaseous dry deposition in air-quality models, *Atmos. Chem. Phys.*, *3*, 2067–2082, doi:10.5194/acp-3-2067-2003.

M. Aikawa, T. Hiraki, and T. Kobayashi, Hyogo Prefectural Institute of Environmental Sciences, Kobe, Hyogo 654-0037, Japan.

M. Kajino, Meteorological Research Institute, Tsukuba, Ibaraki 305-0052, Japan.

G. Katata and H. Nagai, Japan Atomic Energy Agency, 2-4 Shirakata-shirane, Tokai, Ibaraki 319-1195, Japan. (katata.genki@jaea.go.jp)